Research Article

Yingjiao Chen and Mingder Jean*

Multi-response optimization of friction stir welding using fuzzy-grey system

https://doi.org/10.1515/htmp-2024-0005
received February 01, 2024; accepted March 18, 2024

Abstract: This study reports that a fuzzy logic-based grey system using Taguchi's method provides a reliable approach to the prediction of friction stir welding (FSW), which is capable of improving the multi-response performance of butt welds. Using the grey relational database, a fuzzy logic analysis is carried out. Analysis of variance is used to determine the effect of parameters of multi-response behaviors on butt welds. Meanwhile, multiple responses for multivariables are simultaneously optimized. The experimental results show that the fuzzy logic-based grey system using Taguchi's design reveals the optimal settings of the parameters, which improves the whole properties by more than 28.04%, while the individual properties, such as tensile strength by 13.35%, bending strength by 1.91%, impact strength by 1.05%, and hardness by 0.26%, when compared with the best test in orthogonal arrays. Based on experimental validation tests, excellent agreement between model predictions and experimental results is shown. Notably, the intelligent method proposed is applied to butt welds, and the results of the implementation of fuzzy logic based grey system using Taguchi's design proved its feasibility and effectiveness with respect to the improvement of the mechanical properties of FSW.

Keywords: friction stir welding, fuzzy logic, grey rational analysis, multiple responses, optimization

1 Introduction

The relatively unique process of friction stir welding (FSW) was first developed in the early 1990s [1,2]. This technique uses a non-consumable rotational milling tool to generate heat of friction and to deform the material, while it is in a solid state to influence the formation of the joint, making it one of the more significant and potential new welding techniques. In recent years, the development of lightweight advanced components has been a major research project, especially for the automotive and aerospace industries. Yet, light metal alloys can be problematic for fusion and resistance welding due to their lack of structural transformation and excellent thermal and electrical conductivity in the solid state [3,4]. There are some hard to weld materials such as aluminium, magnesium, copper, steel, titanium composites and dissimilar materials, those alloys mentioned above are considered unweldable by conventional techniques. Thus, the FSW has gained attention as an attractive alternative to conventional fusion welding in the case of joining metals that are difficult to weld, especially aluminum metal alloys [5–8]. However, the unique nature of FSW offers several advantages, including nondepletable tools, no filler material, and no shielding gas for making the welds when compared to fusion welding methods, because drawbacks from liquid cooling-related imperfections can be avoided [9,10]. Some problems such as porosity, solute redistribution, and solid-state cracking do not occur during welding. That is, the FSW technique is effective in reducing welding defects such as porosity, grain boundaries, alloy segregation, and cracks, which mostly occur during the joining by fusion welding. Based on the discussion above, FSW has received a lot of attention for its robust solid-state and environmentally preferable joint process. But FSW involves some unique defects including insufficient weld temperature, extensive distortion during the welding process, and ripples along the weld bead, etc [11,12]. Therefore, there is a strong motivation to focus on developing better ways to address the shortcomings of the FSW. Several methods have been efficiently implemented by researchers in order to provide an effective solution to the unique defects of the FSW process. Most researchers have carried out a lot of work on material flow, microstructure formation, and mechanical properties of welded joints by friction stirring. Barcellona et al. [13] studied the structure of aluminum alloy stir friction welding. Butt joints of two different materials were studied metallurgically. Lee et al. [14] investigated the influence of the friction stir processing zone on the material flow behavior

* **Corresponding author: Mingder Jean**, College of Arts and Designs, Jimei University, 185 Yinjiang Rd, Jimei District, Xiamen, 361021, China, e-mail: mdjeam@foxmail.com
Yingjiao Chen: College of Design and Innovation, Fujian Jiangxia University, Fujian, China

subjected to rotating tool activity. The choice of process parameters and weld tool geometry was mainly influenced by the material flow behavior. Although many of the problems in FSW welding focus on the mechanical properties of the stirred zone (SZ) of the weld, there has been great success for welding using a series of materials such as aluminum, copper, titanium, steel, magnesium, and composites [15–23]. Recently, some empirical models of controlled manufacturing processes have been developed to obtain better information for solving problems [24–26]. But, it exists with significant nonlinearities, some inputs and outputs as well as stochastic variations. Currently, many studies have focused on the optimization of individual properties during manufacturing process [27–29]. Elangovan et al. [30] extended a numerical form to predict the elongation strength of friction stir-welded joints of AA 6061 by friction stir parameters such as axial load, tool pin profile, traverse speed, and tool rotation speed. Bayazid et al. [31] used Taguchi's method to optimize the parameters of the process for the manufacturing of the butt joints of 6063–7075 aluminum alloy. Kadaganchi et al. [32] developed a mathematical model using process parameters and tool geometry to predict the response, in terms of yield strength, tensile strength, and ductility, for friction stir welds in AA 2014-T6 aluminum alloy. As mentioned earlier, a lot of researches have been conducted around the influence of FSW parameters and tool geometry on mechanical properties and microstructural characteristics [33,34]. Briefly, there are good results for all of these studies, regardless of other metrics. In contrast, individual indicators of performance are often optimized at the expense of decreasing other indicators. It is because of the complexity and conflicts between indicators. However, due to the nature of noise and complex multivariable systems, the relationship between parameters and individual or multipurpose performances by FSW is not fully understood [35–37]. It involves a certain degree of imprecision and highly subjective availability of data, which are the characteristics that make it a challenge to understand the mechanism of FSW with uncertainty and to further develop a reliable explanation. Accordingly, an innovative model is proposed to investigate the linkage between multiple responses and the various individual responses, which offer a better understanding of the mechanical properties of the joint.

Several well-established methods in multi-response characteristics for modeling and optimization by various empirical and mathematical models such as probability and statistics, desirability function, Taguchi loss function, and grey systems theory employed in studies of non-deterministic systems have proposed in the literature [38–41]. Shaik et al. [42] investigated the multi-objective optimization of the FSW to improve the microstructure of aluminum alloys. The effect of tool rotational speed, welding speed, and tilt angle on tensile strength, impact strength, and elongation was investigated using grey relation analysis method. Jain et al. [43] studied the effect of four parameters in the FSW process on the welding quality such as elongation and ultimate tensile strength of dissimilar aluminum alloys. Jagadish et al. [44] proposed a novel optimization algorithm based on fuzzy logic decision support system, which optimizes the process parameters of the GM process. Vijayan [45] performed parameter optimization of AA5083 weld by FSW, which was done on the basis of an orthogonal array that has multiple responses. Venkateswarlu et al. [46] studied the optimization of dissimilar stir friction welding of AA 2219 and AA 7039. The ultimate tensile strength after optimization was 280 MPa and elongation was 11.5%. Senthil et al. [47] investigated a multi-objective optimization technique based on response surface methodology to optimize the parameters of FSW process for AA6063-T6 pipes. Welded joints with excellent tensile properties, including maximum yield strength, ultimate tensile strength, and maximum elongation, were obtained. Ojo and Taban [48] proposed a robust multi-response optimization of process parameters for stir friction spot welding using a combination of both Taguchi-based gray relational analysis and principal component analysis. Puviyarasan and Senthi [49] undertook a multi-objective optimization of the stirring friction process parameters using a Taguchi-based desirability function approach to fabricate AA6061/B4Cp composites. Also, Dinesh Kumar et al. [50] studied multi-response optimization to optimize tensile strength, yield strength, and elongation. Based on the analysis of the aforementioned literature, the optimization of the individual response of FSW was carried out for different light metal alloys by process parameters. For most of the research works on FSW, the multi-response was done by considering the response individually [51–54]. Moreover, there is further challenge that multiple response indicators are a combination of weights for multiple individual targets, each of which is difficult to be determined. Consequently, there is a strong need to optimize the performance of multiple responses with an understanding of the different characteristics of the mechanical properties of FSW butt joints.

In summary, as described by previous researchers, they cannot effectively offer sufficient information from the effects of individual factors on the responses, and much less address the issues that are related to the weighting of multiple responses. Unfortunately, the weights assigned by

decision makers in much of the literature are usually used as an indicator of the relative importance of each subresponse among multiple responses, which leads to great uncertainty and irrationality. Overall, all of the aforementioned publications concerning the prediction and optimization using fuzzy logic based on Taguchi's method that explores multi-objective properties are limited [55–62]. However, instead of mathematically analyzing the properties of uncertain systems, grey systems theory uses grey relational analysis to approach multi-objective behavior, whereas the relationship between various in-process performance indexes in FSW is nonlinear. Because the grey system cannot solve the problem of nonlinearity for the FSW process, an integrated system based on Taguchi's design that improves the shortcomings of grey system theory by fuzzy logic reasoning has the potential to solve the multi-objective problem in the FSW process [63–65]. This study attempts to optimize multiple responses using fuzzy logic analysis coupled with grey system based on Taguchi's design and further derives a set of parameters for the FSW process that improves the mechanical properties of butt welds.

In this study, an effective solution to the multi-response problem is proposed and multi-response properties including tensile strength, bending strength, hardness, and impact strength were explored using fuzzy logic along with grey system based on Taguchi design. An inference procedure was conducted where each response was performed simultaneously on the weights of the multi-response attributes, and the weights were further integrated and converted into an index of multi-response performance. However, fuzzy logic control based on an inference engine with an "IF-THEN" rule database was developed to solve the weighting problem that promises to make it more effective when combined with the grey relational analysis based on Taguchi's design for multi-response optimization.

2 Experimental method

2.1 Materials and preparations

The butt welding is carried out using stir friction welding on a vertical milling machine by an Makino BGII J-70. As shown in Figure 1, the three welding tool configurations utilize tool pins and tool shoulders with different geometries, such as those made of stainless steel. The diameter of the shoulder is 19 mm, while the pins are three different functional types of steels in Table 1. The lengths of the pin

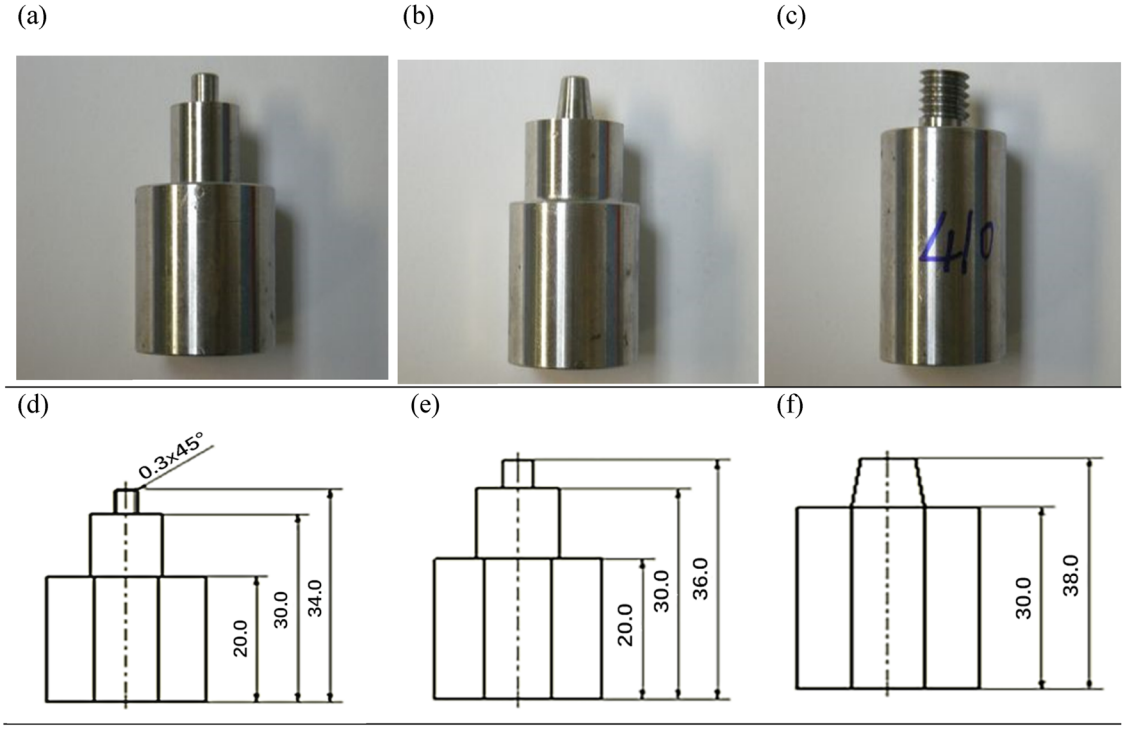

Figure 1: Drawing the configuration of tool pins and shoulders in various geometries made of stainless steel: (a and c) straight cylindrical type, (b and e) tapered type, and (c and f) cylindrical threaded type with geometry and dimension.

Table 1: Control factors and their levels for butt joints

Symbol	Controllable factors	Level 1	Level 2	Level 3
A	Backing plate	Copper	Carbon steel	—
B	Materials of pin	Stainless (410)	Anti-heatsteel (A-600)	Medium carbon steel (S45C)
C	Length of pin (mm)	4	6	8
D	Profiles of pin	Straight cylindrical type	Taper type	Cylindrical-screw type
E	Dwell time (s)	5	15	25
F	Rotation speed (rpm)	560	900	1800
G	Traverse speed ($mm \cdot min^{-1}$)	50	100	150
H	Tilt angle (degree)	0	2.5	5

are 4, 6, and 8 mm, slightly less than the thickness of the welded plate. A 6061 aluminum alloy is used. The dimensions of the aluminum alloy plate are 140 cm long, 70 cm wide, and 0.8 cm thick, and the axial force of the tool is 4–8 kN for welding. As shown in Figure 2, the FSW operation flow chart is divided into five stages. The procedure of stir friction welding includes: start to activate the rotation of the spin, the spin to be further plunged into the plate to be welded, the welding operation to be completed, then the spin to be pulled out of the plate, and the work to be finished. The microhardness tests are carried out using an AVK-C1 hardometer manufactured by Mitutoyo. The tests are carried out on the entire butt weld, where the distribution of hardness is measured mainly in the stirring zone, and 20 points are tested. In addition, tensile tests are conducted in accordance with ASTM E8/E8M standard methods using an Instron tester (MTS 800) with a crosshead speed of $1.67\ mm \cdot s^{-1}$. The tensile properties of the welded areas using three tensile specimens are evaluated. The fractured surface of the specimen is examined using the JEOL JSM-6700F, and metallographic examination of the weld of the scanning electronic microscope (SEM) is taken. Also, the bending properties of the specimen are tested using the MTS 800 tester. The test is carried out on the SZ of aluminum alloy sheets on the butt welds by the use of a compressive bending method. For each of the tests, notched three-point bending specimens with rectangular cross-section samples are used, which were examined by SEM to look at the fracture behavior generated by different bending forces. Besides, the impact absorbed energy of the weld beads is tested using a SATEC impact machine with an impact angle of 135 degrees. The size of the specimen is 7.5 mm × 10 mm × 55 mm. By aligning the notch of the specimen with the center of the support table and simultaneously striking the specimen with a hammer, the impact properties of the specimen can be obtained based on ASTM E23 specification.

2.2 Experimental design

FSW is a solid-state joining technique in which a special tool generates heat by friction on the contact surface that induces deformation of the material surface. When using the FSW technique to welding, the process has a large number of parameters that need to be controlled in order to avoid some defects affecting the mechanical properties. However, the FSW process involves many process parameters that affect the quality of the welding joints. Since many factors can be evaluated by a small number of experiments, the Taguchi method with orthogonal arrays is implemented. Its design provides a powerful and

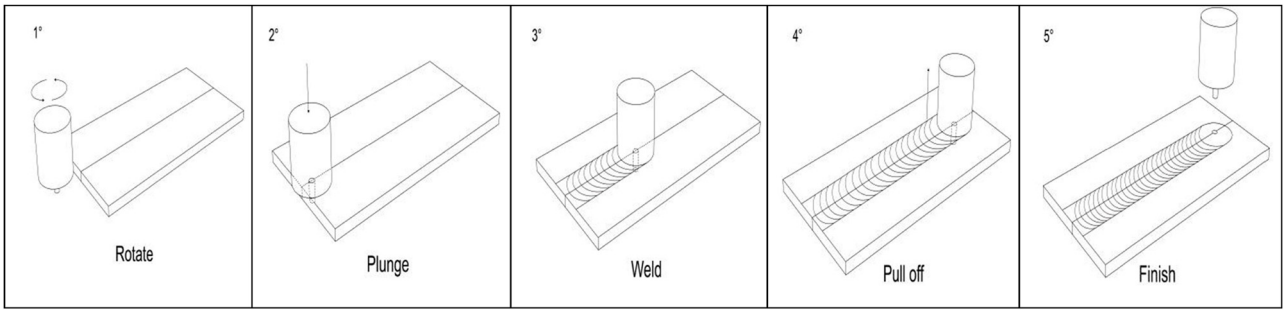

Figure 2: Flow chart of the operation of FSW at five stages, namely, rotation, plunge, welding, pull-out, and finish.

efficient way to design products that are reliable to operate consistently and optimally under various conditions [63]. In addition, its array is balanced so that each factor can be analyzed individually, where it greatly reduces the variance of the experiment and controls the optimal setting of the parameters. An L18 ($2^1 \times 3^7$) table is used. As shown in Table 1, there is one 2-level factor A and seven 3-level factors, which are divided into orthogonal arrays. These are listed in Table 2 along with the alternative levels used in the experiment. A special form of the transformation of the response is used, the so-called signal-to-noise ratio (S/N), from the field of communication engineering. In this study, larger-the-better type is involved in butt welds. The loss function-based S/N ratio is calculated as

$$\mathrm{S/N} = -10\mathrm{Log}\left[\frac{1}{n}\left(\sum_{i=1}^{n}\frac{1}{y_i^2}\right)\right]. \quad (1)$$

The S/N ratios were calculated based on equation (1), and their mean values and standard deviations for each of the parameters of the process are summarized in Table 2. Each test was replicated three times for each response characteristic, and the S/N ratio of the tests was analyzed by analysis of variance (ANOVA) to identify the significant factors that contributed to each quality characteristic. These factors were then considered to analyze the predictors of fuzzy-grey system.

3 Multi-response optimization of the butt welds

3.1 Grey relational analysis

Grey system theory was initially proposed by Deng in 1982 as an effective method in solving the uncertainty, incomplete and complexity information have been proposed [64]. This theory conducts relational analysis and model construction on unclear information and incomplete data within a system and also investigates the system by prediction and decision-making methods. By means of system relational analysis along with model building through prediction or decision analysis, the grey relational analysis is utilized to address the non-linear relationships among multiple responses. This method analyzes a process that has unknown or incomplete information about the effect of parameters on the responses. The grey relational coefficient is calculated to identify the relationship between the reference sequence and the comparability sequence. There are many problems involving the use of estimated performance for the manufactured products with various quality characteristics, such as different units, types and importance, and different quality characteristics, which often lead to a great deal of uncertainty and unreasonableness.

Table 2: Experimental data, normalized value of various properties, including tensile (*T*), bending (*B*), impacting (*I*), and hardness (*H*) properties, with one 2-level factor and seven 3-level factors based on orthogonal arrays for the butt welds

EXP	A	B	C	D	E	F	G	H	Experimental data of mean and st.dev								Normalization			
									T (MPa)		*B* (MPa)		*I* (MJ·m^{-2})		*H* (HV)		*T*	*B*	*I*	*H*
1	1	1	1	1	1	1	1	1	91.33	5.03	22.67	2.89	22.42	0.28	79.05	10.08	0.065	0.103	0.305	0.731
2	1	1	2	2	2	2	2	2	170.00	6.93	42.33	3.51	29.5	0.43	80.43	7.79	0.738	0.654	0.458	0.815
3	1	1	3	3	3	3	3	3	133.33	3.79	28.00	1.00	13.49	1.92	81.28	6.47	0.424	0.252	0.111	0.867
4	1	2	1	1	2	2	3	3	95.33	2.08	22.00	0.00	16.27	0.33	76.61	19.23	0.100	0.084	0.171	0.582
5	1	2	2	2	3	3	1	1	136.33	0.58	36.33	1.53	15.72	0.52	82.87	9.91	0.450	0.486	0.159	0.963
6	1	2	3	3	1	1	2	2	189.33	2.08	42.33	2.52	54.47	6.33	81.70	4.14	0.903	0.654	1.000	0.892
7	1	3	1	2	1	3	2	3	101.00	1.73	26.00	1.00	19.81	0.66	84.59	11.10	0.148	0.196	0.248	0.932
8	1	3	2	3	2	1	3	1	147.33	2.52	33.00	2.65	54.21	1.11	80.86	14.21	0.544	0.392	0.994	0.841
9	1	3	3	1	3	2	1	2	175.33	3.22	41.00	1.73	51.35	2.41	83.44	7.33	0.783	0.617	0.932	0.998
10	2	1	1	3	3	2	2	1	97.67	1.16	25.00	0.00	27.84	0.90	81.60	16.89	0.120	0.168	0.422	0.886
11	2	1	2	1	1	3	3	2	83.67	0.58	19.00	1.73	11.5	1.33	94.14	6.27	0.000	0.000	0.068	0.351
12	2	1	3	2	2	1	1	3	200.67	0.58	54.67	0.58	41.64	1.49	75.95	9.53	1.000	1.000	0.722	0.542
13	2	2	1	2	3	1	3	2	93.33	1.53	21.33	0.58	8.37	0.11	99.90	3.49	0.083	0.065	0.000	0.000
14	2	2	2	3	1	2	1	3	139.33	2.08	44.33	1.53	45.6	0.89	81.38	12.92	0.476	0.710	0.808	0.873
15	2	2	3	1	2	3	2	1	154.67	5.13	40.00	0.00	46.88	1.82	85.60	4.38	0.607	0.589	0.835	0.870
16	2	3	1	3	2	3	1	2	102.33	2.31	22.33	0.58	8.66	0.23	81.72	19.15	0.159	0.093	0.006	0.893
17	2	3	2	1	3	1	2	3	172.33	2.08	52.33	0.58	53.81	2.11	84.03	15.10	0.758	0.934	0.986	0.966
18	2	3	3	2	1	2	3	1	95.00	4.36	20.67	0.58	20.05	2.46	87.32	7.78	0.097	0.047	0.253	0.766

Table 3: Desired deviation, the grey relational coefficient, index of fuzzy inference, and S/N ratio of each L18 orthogonal array

No. of tests	Desired deviation				Relational coefficient				Index of fuzzy-grey inference	S/N ratio
	ΔT	ΔB	ΔI	ΔH	$\xi 1$	$\xi 2$	$\xi 3$	$\xi 4$		
1	0.935	0.897	0.695	0.269	0.349	0.358	0.418	0.650	0.396	−4.023
2	0.262	0.346	0.542	0.185	0.656	0.591	0.480	0.730	0.615	−2.111
3	0.576	0.748	0.889	0.133	0.465	0.401	0.360	0.789	0.469	−3.288
4	0.900	0.916	0.829	0.418	0.357	0.353	0.376	0.545	0.364	−4.389
5	0.550	0.514	0.841	0.037	0.476	0.493	0.373	0.932	0.541	−2.668
6	0.097	0.346	0.000	0.108	0.838	0.591	1.000	0.823	0.734	−1.343
7	0.852	0.804	0.752	0.068	0.370	0.384	0.399	0.880	0.436	−3.605
8	0.456	0.608	0.006	0.159	0.523	0.451	0.989	0.759	0.614	−2.118
9	0.217	0.383	0.068	0.002	0.698	0.566	0.881	0.996	0.702	−1.537
10	0.880	0.832	0.578	0.114	0.362	0.375	0.464	0.815	0.430	−3.665
11	1.000	1.000	0.932	0.649	0.333	0.333	0.349	0.435	0.335	−4.750
12	0.000	0.000	0.278	0.458	1.000	1.000	0.642	0.522	0.789	−1.029
13	0.917	0.935	1.000	1.000	0.353	0.349	0.333	0.333	0.339	−4.698
14	0.524	0.290	0.192	0.127	0.488	0.633	0.722	0.797	0.653	−1.851
15	0.393	0.411	0.165	0.130	0.560	0.549	0.752	0.794	0.615	−2.111
16	0.841	0.907	0.994	0.107	0.373	0.355	0.335	0.824	0.418	−3.788
17	0.242	0.066	0.014	0.034	0.674	0.884	0.972	0.936	0.794	−1.002
18	0.903	0.897	0.747	0.234	0.356	0.344	0.401	0.681	0.400	−3.979

Accordingly, the relationship between various performance indexes in the FSW process tends to be uncertain, imprecise, or qualitative decision-making problems. The grey relational analysis has the superior features of fewer data sets of possible parameter design for comparison and a high level of efficiency to reach the optimal solution. For these purposes, grey relational analysis based on the grey system is used for solving the complicated interrelationships among the multiple responses. Depending on their different objectives, the raw values of the responses that were collected during the experimental runs were converted to values between 0 and 1. The method utilizes an objective function called normalization, which reflects the actual value of each response in equations (2) and (3). The rules for normalization are calculated for multiple quality characteristics, such as larger-better and nominal-better types:

$$\bar{y}_i(k) = \frac{\max[x_i^{(0)}(k)] - x_i^{(0)}(k)}{\max[x_i^{(0)}(k)] - \min[x_i^{(0)}(k)]}, \tag{2}$$

$$\bar{y}_i(k) = 1 - \frac{|x_i^{(0)}(k) - \hat{x}|}{\max\{\max[x_i^{(0)}(k)] - \hat{x},\ \hat{}x - \min\lceil x_i^{(0)}(k)\rceil\}}, \tag{3}$$

where $x_i^{(0)}(k)$ is the control variable, the ideal value is $\hat{x}$, $\bar{y}_i(k)$ is the normalized value, $y_i(k)$ is the kth response of the ith experiment, min $[x_i^{(0)}(k)]$ is the minimum value of $x_i^{(0)}(k)$, and max $[x_i^{(0)}(k)]$ is the maximum value of $x_i^{(0)}(k)$, i = 1, 2, 3, the number of experiments and k = 1, 2, 3, the number of responses. As listed in Table 4, four different measures were considered in the normalized procedure, namely, tensile, bending, impact, and microhardness properties. On the basis of the values of normalization, the grey coefficient is calculated using equations (2) and (3). These results are given in Table 4. The grey relational coefficient (ξ) is calculated as follows:

$$\xi_i(\bar{y}_i(k), \bar{y}_j(k)) = \frac{\Delta \min + \delta \Delta \max}{\Delta_{oi}(k) + \delta \Delta \max}, \tag{4}$$

where $\Delta_{oi}(k) = |\bar{y}_0(k) - \bar{y}_i(k)|$, i = 1, 2...., m; k = 1, 2,...p. It is the absolute value of the sequence $\bar{y}_{i0}$ and $\bar{y}_0$ at the kth difference. Δ max = $\max_{\forall k} \max_{\forall i} \Delta_{oi}(k)$ is the maximum distance between the curve reference and the test sequence, and Δ min = $\min_{\forall k} \min_{\forall i} \Delta_{oi}(k)$ is the minimum distance between the curve reference and the test sequence. δ is a user-selectable coefficient, and the value of δ is defined in the range between 0 and 1; commonly, it is set as 0.5.

3.2 Fuzzy inference systems

In 1965, L. Zadeh first introduced the concept of fuzzy sets, which marked the birth of fuzzy mathematics [65]. It is based on two-binary logic, which applies the original logic and mathematics that provide a solution to the difficulty of describing and dealing with many ambiguous matters in the real world. It uses inference principles to solve the problems with several rules that come from experienced

Table 4: Response table of means for multi-response properties

No. of level	Control factor and their levels							
	A	B	C	D	E	F	G	H
Level 1	−2.787	−3.144	−4.028	−2.969	−3.259	−2.369	−2.483	−3.094
Level 2	−2.986	−2.843	−2.417	−3.015	−2.591	−2.922	−2.306	−3.038
Level 3	0.000	−2.672	−2.215	−2.676	−2.810	−3.368	−3.870	−2.527
Effect	0.199	0.473	1.814	0.340	0.668	1.000	1.564	0.567

operators and experiments, rather than general mathematical models, so that the linguistic implementation is done faster. However, fuzzy logic control is the integration of human intuition and experience into the control system by establishing a series of rule bases, which further use fuzzy reasoning to find out the mapping relationship between input and output by fuzzy inference method so that the control of the system can be realized. In this study, an index of multi-response performance is derived by fuzzy theory, and its structure can be divided into input unit, fuzzy decision unit, and output unit, while fuzzy decision unit includes fuzzy interface, fuzzy rule base, fuzzy inference engine, and defuzzification interface. It interacts by interpreting the relationship between inputs and responses through a fuzzy rule base that consists of a set of IF-THEN rules. A fuzzy rule is a collection of linguistic statements that describe how a fuzzy inference-based system should categorize the decisions of inputs or control outputs. A database of fuzzy rules is several sets of "IF-THEN" rules, where the "IF-THEN" rules are as follows: for a R_i rule,

$$R_i : \text{If } x_1 \text{ is } A_{i1},\ x_2 \text{ is } A_{i2},\ldots,\ \text{and } x_s \text{ is } A_{is},\ \text{then } y_i \text{ is } C_i,\quad i = 1,\ 2,\ldots,\ M, \tag{5}$$

where M is the total number of fuzzy rules, x_j (j = 1, 2,...., s) are the input variables, y_i are the output variables, and A_{ij} and C_i are the fuzzy sets characterized by membership functions $\mu_{A_{ij}}(x_j)$ and $\mu_{C_{ij}}(y_i)$, respectively. As shown in Figure 3, a procedure of fuzzy inference using a Mamdani fuzzy system with two inputs, an inference engine with a knowledge base, and an output where the knowledge base has two "IF-THEN" rules, while the defuzzification interface is calculated using the center of gravity method.

Based on the Mamdani implication method of inference reasoning for a set of disjunctive rules, the conjugate "and" of the rule antecedent takes the minimum value of the t norm (Min). In this study, grey correlation degree that weights the grey relational coefficient of the responses for each system in the fuzzy logic system was evaluated. It evaluates the outcome of a fuzzy rule using the given input information. For instance, the output of the ith rule in equation (6) after inference operation is given by

$$w_i = \underset{i}{\text{Min}}(\mu_{A_{i1}}(x_1), \mu_{A_{i2}}(x_2),....,\mu_{A_{is}}(x_s)), \tag{6}$$

where w_i is called the firing strength of the ith rule. In addition, the results of inference for various rules are

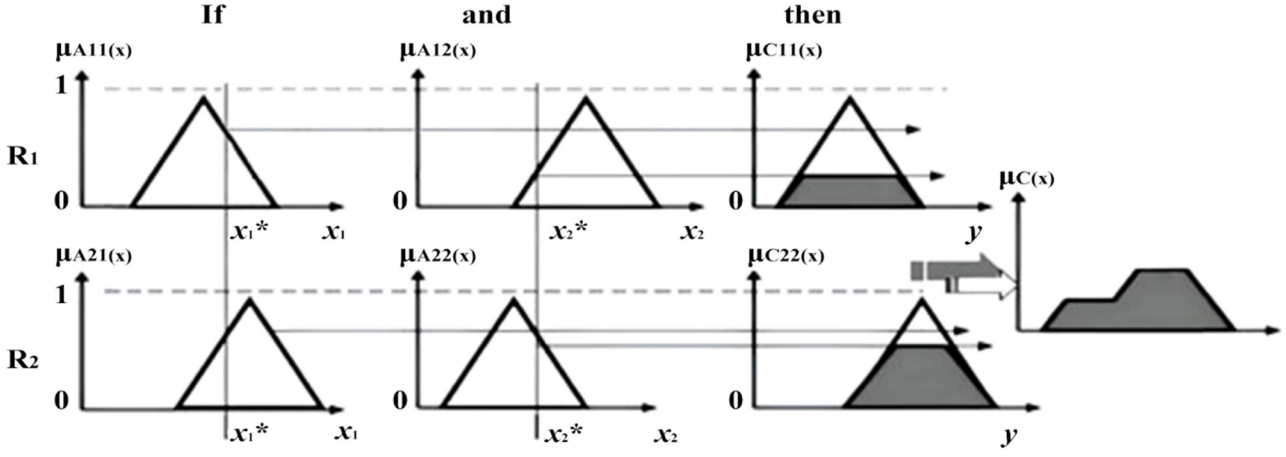

Figure 3: Example of fuzzy reasoning using a Mamdani fuzzy system with two inputs and a knowledge base with two "IF-THEN" rules.

aggregated by applying s-norm maximum (Max). Accordingly, the aggregated output for the M rules is

$$\mu_{C_i}(\bar{y}_i) = \text{Max}[\underset{i}{\text{Min}}(\mu_{A_{i1}}(x_1), \mu_{A_{i2}}(x_2),....,\mu_{A_{is}}(x_s))], \quad i = 1, 2,..., M. \tag{7}$$

Therefore, the grey relational grade (γ_i) can be expressed as follows:

$$\gamma_i = \sum_{k=1}^{n} \mu_{c_i} \xi_i(\bar{y}_i(k), \bar{y}_j(k)) \quad i = 1, 2,..., n. \tag{8}$$

The fuzzy rule base of the fuzzy inference system that represents eighty-one rules with four input variables, using triangular membership functions, was used. In this work, the gravity method was used in the defuzzification process. The value of the defuzzification is calculated using equation (9), which is referred to as the multi-performance characteristic index (MPCI). The formula to find the centroid of the combined rule outputs, MPCI, is given by

$$\text{MPCI}_i = \frac{\sum_{k=1}^{n} \mu_{c_i} \xi_i(\bar{y}_i(k), \bar{y}_j(k))}{\sum_{i=1}^{n} \mu_{c_i}(\bar{y}_i)}. \tag{9}$$

The yielded value is the final output value obtained from the input variables.

In this study, the four inputs are tensile, bending, impacting, and hardness values; each of the input signals is fuzzily divided into three subsets, namely, small (S), medium (M), and large (L); and the output signals are fuzzily divided into nine subsets, namely, extremely small (ES), very small (VS), small (S), small medium (SM), medium (M), medium large (ML), large (L), very large (VL), and extremely large (EL), as shown in Figure 4. The rule database in this study contains four input variables, each of which is divided into three fuzzy sets and one output with nine fuzzy sets, which creates a total of "IF-THEN" rule databases to form a fuzzy inference engine, which can be computed using equations 5–9. A fuzzy logic with eighty-one rules is constructed. Figure 5 shows the graphical programs and findings for Test 1 using Matlab2021, where the rows denote the 81 rules and the columns denote the four input variables. Figure 5 shows that the subsets of triggers are ES, VS, S, SM, M, and ML, which shows the operation of the four input signals on the whole rules, and there are eight rules that are triggered. By applying the logic rules and Mamdani inference procedure, several logic rules can be triggered, which give the fuzzy linguistic value of the output response. A fuzzy inference system with the rule-base input containing grey relational coefficients of tensile, bending, impact, and hardness values is analyzed. Using the first test as an example, the four input signals are 0.349 for the tensile value, 0.358 for the bending value, 0.418 for the impact value, and 0.650 for the hardness value, respectively, which are computed by the fuzzy inference engine. The results of rules 2-3, 5-6, 10-12, 14-15, 28-29, 31-32, 37-38, and 40-41 of the reasoning procedure are fired simultaneously. As shown in Figure 5, 16 rules of the 81-rule database were triggered, which are highlighted in the dark area of the right foot, i.e., the fuzzy set of the dark area. As a result, the calculated MPCI is 0.396, which is displayed in the upper-right corner in Figure 5.

As noted in equation (9), the SN ratios based on the results of the fuzzy grey relational analysis are calculated for multiple characteristic index (MPCI) in terms of the-larger and the-better type, as follows:

$$\varsigma_i = -10\text{Log}\left(\frac{1}{\text{MPCI}_i}\right) i = 1,2,3,\ldots, n, \tag{10}$$

where MPCI_i is the indicator of fuzzy-grey relational grade, and ς_i is the S/N ratio of multi-response performance. In short, the larger the SN ratio, the better the overall quality performance is. That is, the higher this S/N ratio is, the more the

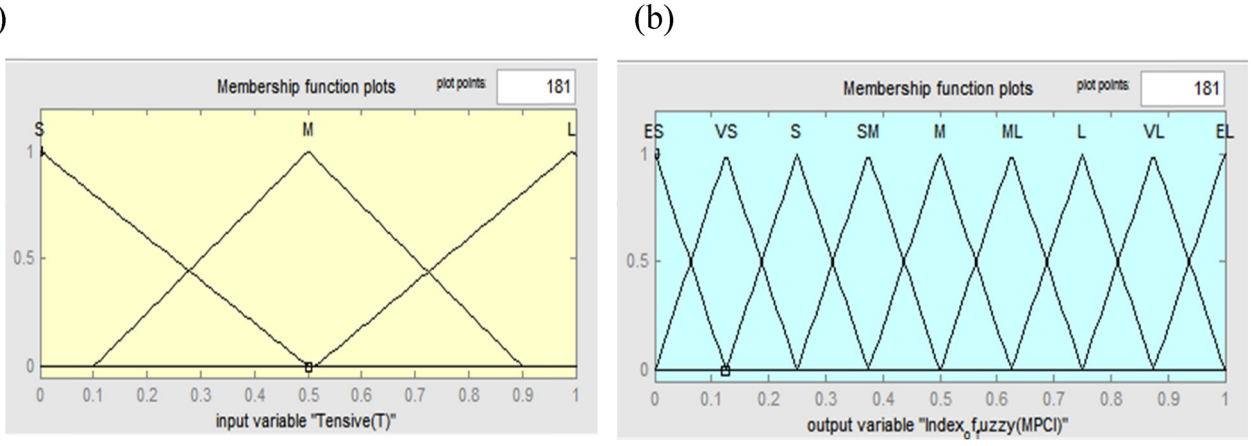

Figure 4: Membership functions of the four inputs with the coefficient of the grey system (a) and the output of the index of fuzzy-grey system (b).

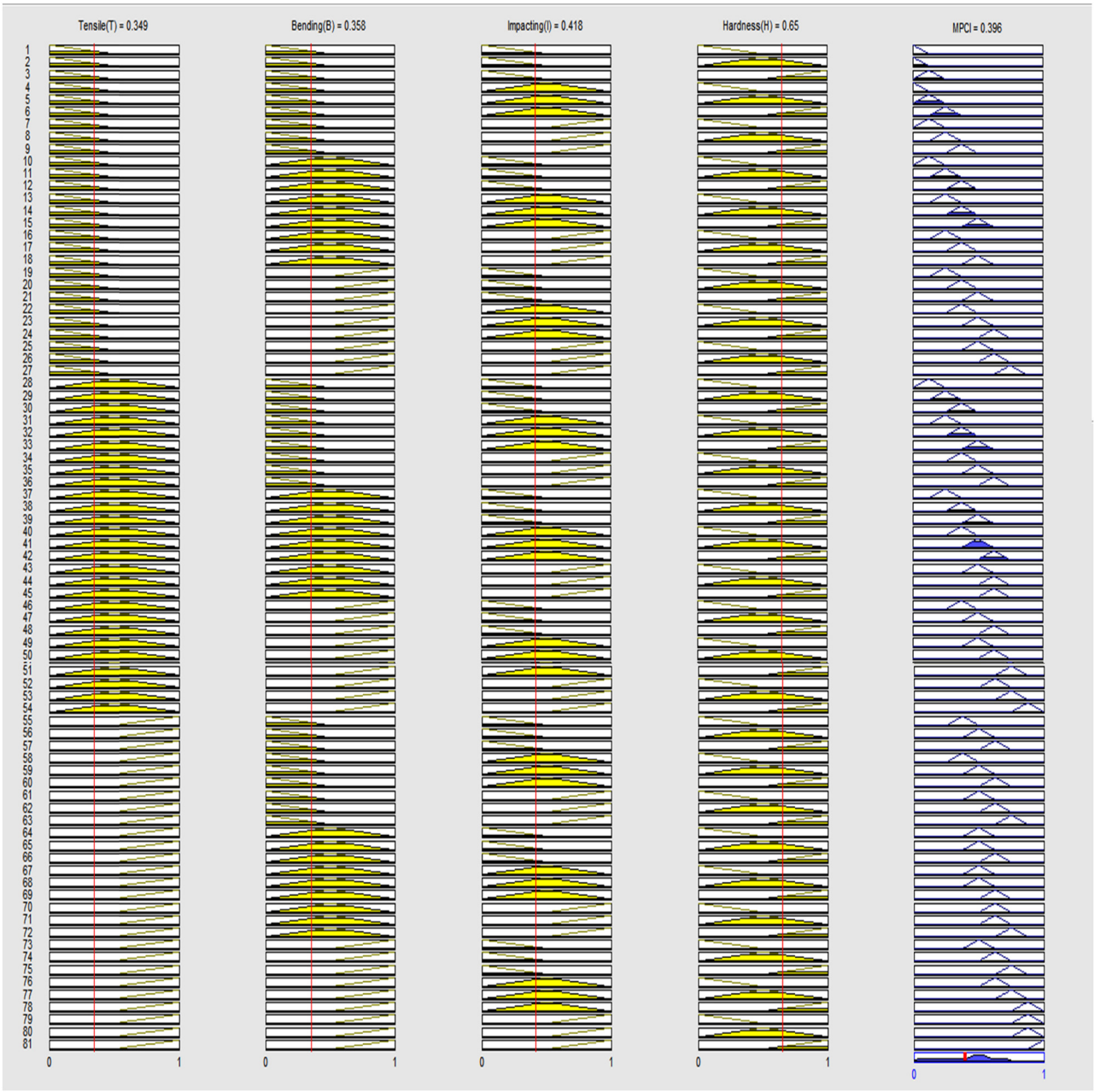

Figure 5: Four inputs with the grey relational coefficient and the output of fuzzy logic system for the multi-response performance by forming eighty-one "IF-THEN" rules in the fuzzy system.

FSW system gets to work as it does not affected by the noise factor. In addition, the system is more resistant to noise.

3.3 ANOVA

This experiment applies the audio concept of S/N to a multiple-variable design. The S/N ratio measures the level of spraying performance as shown in Table 3. It is estimated by the S/N ratios on whether a large response; a smaller response or an on-target response is desirable [6]. The purpose of ANOVA, which it performs with the mean sums of squares, is to separate and then compare such variabilities. ANOVA performs the factor effect from S/N ratios of the averaging of certain observations. Nonetheless, we use ANOVA when appropriate to determine if the effect of a particular factor on the responses or its variability is significant. ANOVA identifies which influencing

factors have the largest impact on the average level of performance and the variability of the responses in terms of the predefined experimental results. These important factors will be considered during the process optimization for surface response design.

4 Experimental results and discussion

4.1 Multi-response performance and factorial influenced analysis of butt welds

The optimal FSW process for the welds is expected to yield the desired performance of the multi-response properties. Table 2 shows the findings of the whole tests. The results of the experiments in 18 groups were compared in terms of the different characteristics such as tensile (*T*), bending (*B*), impacting (*I*), and hardness (*H*) that could be observed. The L12 specimen showed the highest level of tensile and bending, the L8 specimen revealed the highest level of impacting, and the L16 specimen gave a desirable level of hardness. Clearly, due to the different characteristics of FSW welds, no remarkable tendency of the overall tested results could be found while taking into account several characteristics simultaneously. Accordingly, a method that addresses the problem of multiple responses is needed. In the study, the aforementioned problem was handled by a fuzzy-grey system based on Taguchi design, and satisfactory results could be obtained. The results of the 18 sets of tests conducted according to the required multi-response by using the control factors and their levels for FSW in the Taguchi design are shown in Table 2. The normalization of individual responses was calculated using the larger and better types, while based on the grey system and further calculating the grey relational degree as shown in Tables 2 and 3. Using the large-and-better types, such as the responses shown in Tables 2 and 3, with calculating the normalization of each response, the grey system is used as the basis for further calculating the degree of grey relativities. The properties of tensile and bending of the stirred weld at test 12 give values close to 1, whereas the values of the impact properties at test 8 and the hardness properties at test 16 are relatively close to 0. The calculated values obtained above are close to the maximum values; however, they are not exactly in the same test. Therefore, the stirred welds under these conditions do not fulfill the industrial requirements. The values of tensile, bending, impacting, and hardness of the stirred layer in test 17 are close to the ideal value, and the value is close to 1 in the overall tests, which shows that the value of the grey correlation performance index deduced by the fuzzy inference engine is also close to 1. Meanwhile, the S/N ratio has a higher value, which shows that the stirred layer has excellent quality characteristics. However, the present experiment was carried out by Taguchi's design, which integrated the fuzzy system with the grey relation so that a set of data was obtained for the confirmation experiment in the optimal test as shown in Table 3. As a result, the performance of the overall quality was better than that of the other 18 groups of tests, and the FSW process was successfully developed here.

4.2 ANOVA

The experiments are calculated on the basis of orthogonal tables, and their mean effects are shown in the response tables that reflect the relative importance of each control level in the multi-response properties. As shown in Table 4, the result of the max–min evaluation shows that the effect of parameter C is the strongest, while that of parameter D is the smallest, which further indicates the relative importance of the parameter to the FSW process. In other words, the greater the effect, the greater the impact on product quality is. The results of the reflected table are shown in Table 4. The optimal levels for each factor where the S/N ratio is larger are A1, B3, C3, D3, E2, F1, G2, and H3. Besides, the parameters that significantly affect the quality performance of this experiment are organized as follows: C, G, F, E, H, B, D, and A. The significance of the S/N ratio of the fuzzy grey predicted values for each parameter still subjects to the ANOVA. An ANOVA test was carried out on the S/N ratio of various quality characteristics so as to determine statistically significant welding parameters [64]. The ANOVA table of the S/N ratio based on the experimental results is shown in Table 3. The results of the ANOVA provide a remarkably clear picture in terms of the effect of each factor on the multiple response characteristics. The percentage contributions of the eight control factors on the multiple response characteristics are shown in Table 5: pin length (factor C), dwell time (factor E), tool rotational speed (factor F), and traverse speed (factor G) are highly significant in affecting the multiple response of the welds, while the backing plate (factor A), pin materials (factor B), pin profiles (factor D), and tilt angle (factor H) are less significant. These significant factors account for almost 90.42% of the experimental variation.

Table 5: ANOVA for multi-response properties

Symbol	Sum of squares	Degree of freedom	Mean square	*F*-test	Contribution percent
A	0.18	1.0	0.178	1.676	0.64
B	0.69	2.0	0.344	3.232	2.48
C	11.85	2.0	5.926	55.734	42.77
D	0.41	2.0	0.203	1.913	1.47
E	1.39	2.0	0.695	6.535	5.01
F	3.01	2.0	1.504	14.147	10.86
G	8.81	2.0	4.403	41.413	31.78
H	1.17	2.0	0.585	5.501	4.22
Error	0.21	2.0	0.106	1.000	0.77
Total	27.71	17.0			100.00

4.3 Grey relational coefficients using fuzzy logic system

As seen in equation (5) all rules listed in Figure 5 are accommodating. To develop an approximate solution for the multi-response properties, similar to Figure 3, the graphical reasoning interface is used to operate using four different grey relational coefficients as input. On the basis of the Mamdani inference method as given in Figure 3, the "IF-THEN" rule databases in the fuzzy controller can be analyzed. As shown in Figure 6, the matrix ($\xi 1 = 0.912$, $\xi 2 = 0.957$, $\xi 3 = 0.996$, $\xi 4 = 0.953$) of the optimal tests based on Taguchi's design can be computed. The tensile value activates 44 rules like 28-81; bending activates 27 rules like 19-27, 46-54, 73-81; impacting value activates 27 rules like 7-9, 16-18, 25-28, 34-36, 43-45, 52-54, 61-63, 70-72, and 79-81; and hardness activates 81 rules like 1-81. As shown in Figure 6, 8 rules such as 44-45, 53-54, 71-72, 79-80 are generated, which are displayed in the dark area of the right foot. The S/N ratio of the fuzzy-grey predictive value is 0.847 db, which is obtained by defuzzification, as shown in Figure 6. We selected the best test 17 when compared to the values of all 17 tests in Table 3. It was found that the fuzzy-grey predicted values had the largest S/N ratio, indicating good multi-response characteristics. That is, the larger the fuzzy-grey prediction, the better the tensile, bending, impacting, and hardness are. Accordingly, it is concluded that the fuzzy-grey system is able to be used for effective predictions for the multi-response properties.

4.4 Fractured property distribution of tensile strength for the butt welds

Table 2 shows the results of the 18 experiments. The tensile strength of the 1st, 11th, and 13th sets was found to be lower, with the average value of 83.67 MPa for the 11th test, while the highest tensile strength was found for the 6th, 9th, and 12th tests, with the average value of 200 MPa for the 12th test. Comparing Figure 7 with the experimental data, the fracture of the 13th set of specimens showed irregular tearing at the center of the weld zone, mainly due to incomplete welding, while the fracture of the 9th set was concentrated at the interface between the weld zone and the base material, indicating that the bonding force of the weld was greater than that of the base material and the weld zone. Most of the lower tensile force, butt weld specimens failed in the weld area, but the exact location of failure is either at the retreating side or at the advancing side, which can be viewed from the surface of the fracture, where the tensile strength of the welded joint is about 60–85% of the parent metal strength of 125 MPa. Figure 7 shows the fracture structure of the joint and the microstructure of the specimen after tensile force. In overall tests, the typical elliptical shape of the nugget area is displayed, and the onion rings on the surface are visible. Figure 7a and b shows the fracture surface of the joint of the 13th trial with the 93.33 MPa tensile sample. As shown at the top-left of Figure 7a, it can be seen that there are obvious defects of ripples and extrusions around both edges of the butt weld. Using a tapered type with a length of 4 mm, due to the fact that the pin is only half of the thickness of the welded plate, saw-tooth fractures are only seen in well-welded areas in the tensile test, while linear fractures are seen in poorly welded areas. As shown in Figure 7b, defects in SEM were found in large grains of voids, oxide contamination, and fracture surfaces. Because the pin is too small, an opened root is visible. It cannot meet the tension support. The central zone of the weld bead is susceptible to fracture in tensile testing. It may be due to coarse grains on the fracture surface along with void-like defects, which can induce the fracture of the butt weld zone. In other words, its failure location is fractured in the center of the weld, which leads to spalling in the zone of the open root due to the lack of metallurgical bonding effect, which limits the weld strength very much. This noticeable decrease in tensile properties may be due to the imperfect stirring effect of the welds that are prepared with shorter pin of the shoulder. Figure 7c shows the fractured surface of the 175.33 MPa in the 9th trial of the joints. Using a cylindrical type with a length of 8 mm, the fracture can be seen at the serrated line of the weld.

As shown at the top-left of Figure 7c, there are no noticeable defects such as elliptical shape, ripples on the welding surface, and the formation of onion rings, as well as welding surfaces that have been fully plasticized. The fracture surface in the tensile test of Figure 7d can be found to be microfine-structured by SEM, and the defects

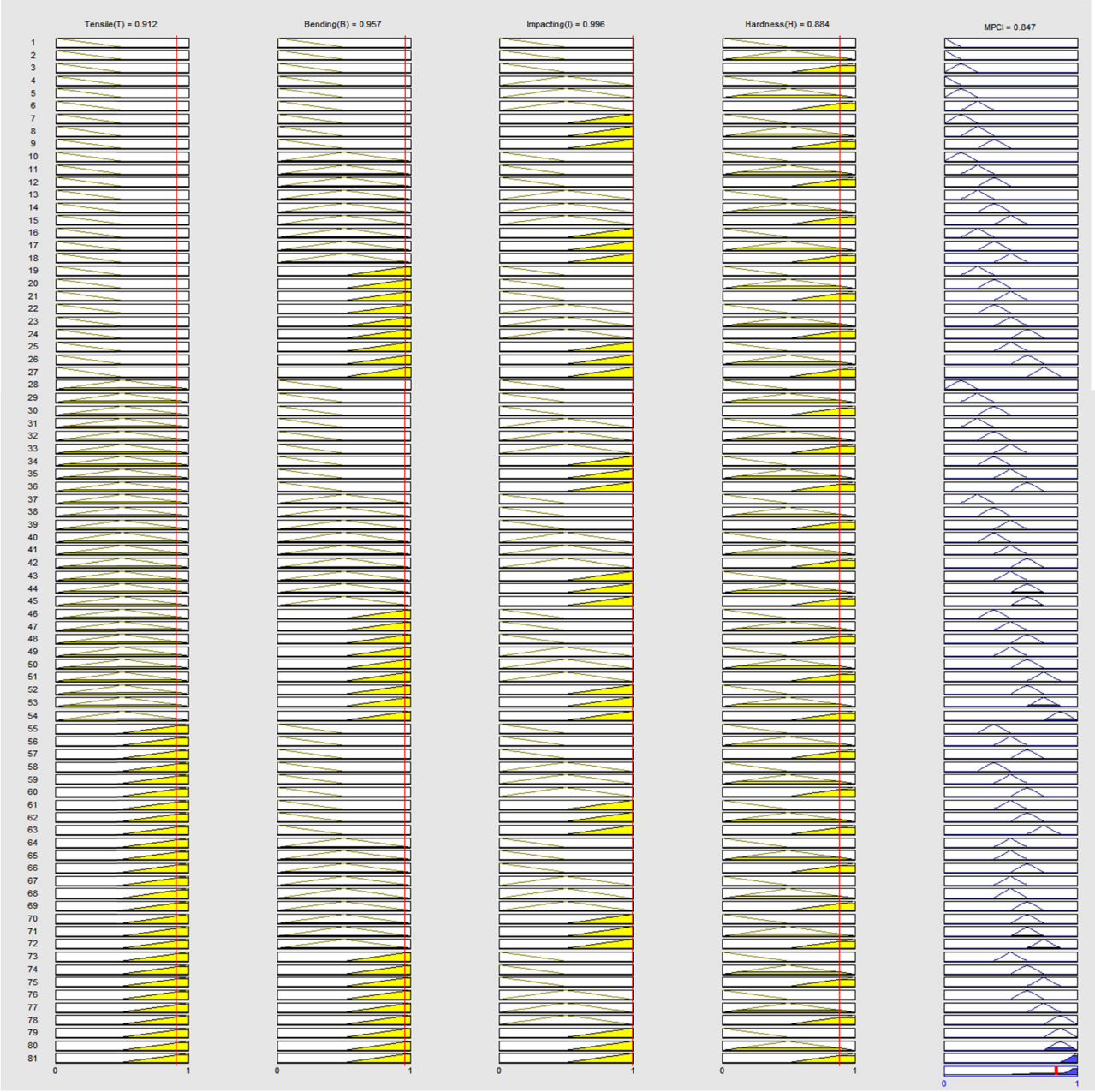

Figure 6: Graphs of the optimal quality of four attributes such as tensile, bending, impacting, and hardness values based on fuzzy-grey prediction, using an "IF-THEN" rule-based inference by fuzzy system.

generated inside the weld are limited, indicating that the failure location and the structure size of that weld are found to be different compared to Figure 7a and b. This means that the weld is fractured in thermo-mechanically affected zone (TMAZ) but not SZ, indicating that the weld is much stronger than the base material. This is mainly due to the fact that the grain size in TMAZ is larger than that in SZ, where the grain size is coarsened.

4.5 Distribution of bending strength for the butt welds

Table 2 shows the results of the 18 experimental groups. The bending strength of the 4th, 11th, 13th, and 18th sets was lower than 22 MPa, of which the 11th set was the lowest, while the bending strength of the 12th, 14th, and 17th sets was higher than 40 MPa, of which the 12th set was

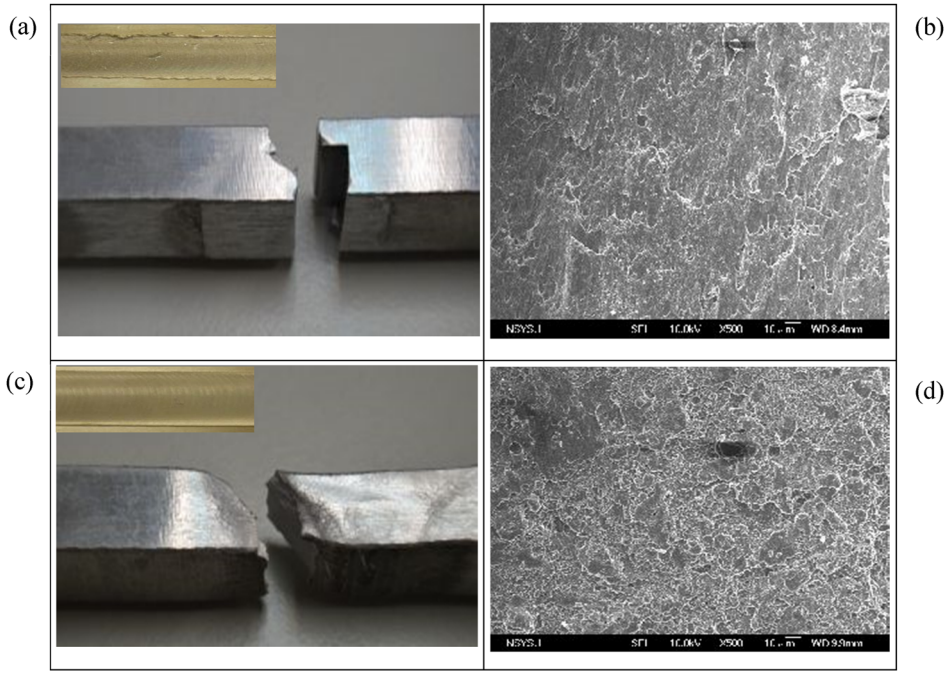

Figure 7: Fractograph and tensile testing of welded joints for test 13 and test 9 tensile specimen using (a, c) the location of fracture and (b, d) microstructures for the traverse-weld specimen.

the highest. The structure of the welded specimen in the bending test is further observed by taking the data of two important groups from Table 2, as shown in Figure 8. The bending diagram of the 11th set is shown in Figure 8a. The complete crack was found in the bottom area of the stir welding, as well as a large cavity in the central part of the melt zone, which could not bear the bending load that led to the fracture of the welding zone. This is attributed to the fact that the dimension of the stirred pin is lower than the thickness of the welded plate, while the bottom zone is not

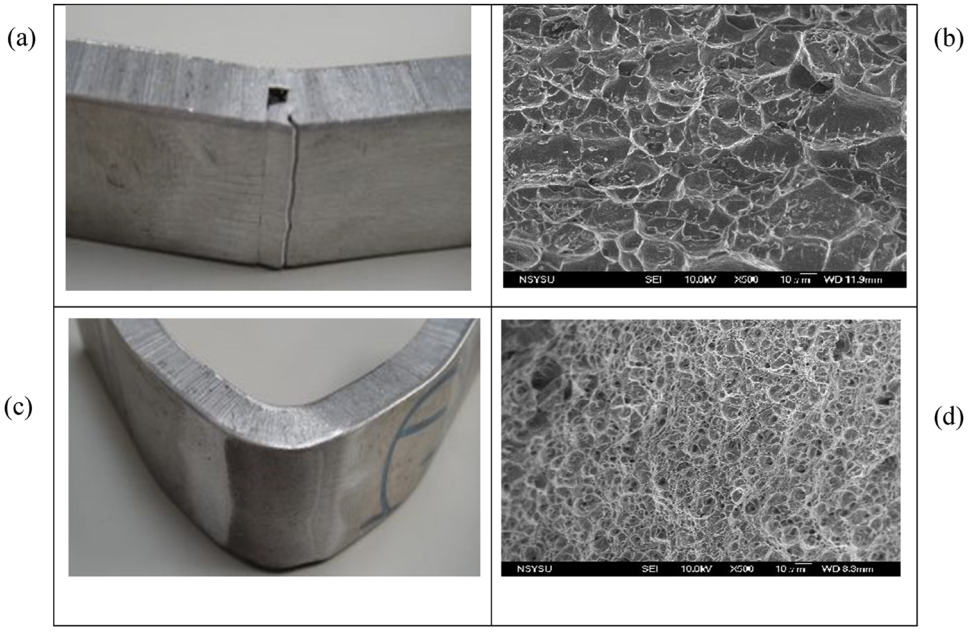

Figure 8: Macrograph of the bending tested specimen with (a and c) macrophotographs of the bending test and (b and d) microstructures for the traverse-weld specimen.

completely welded. As a result, the structure of the SZ is loosened, which leads to cracking by the bending force. In addition, as shown in Figure 8b, the microstructures in SEM are found as grains with diameters over 10 μm in size, some fragments of tearing grains, and large amounts of fracture surfaces. Because there is an open root, only part of the weld is well supported, and therefore, it cannot endure bending forces. It can be seen that the fracture area of the weld bead has larger and looser crystal grains, which can be easily fractured by the force. Conversely, as shown in Figure 8c, the stirring bead was found to be perfectly formed after the bending load, in addition to the bending angle of 50 degrees in the butt zone, where the welds were able to resist the bending load without fracture. Furthermore, as shown in Figure 8d, the microstructure found in SEM is that most of the grains are less than 5 μm in diameter, and a large number of grains with elongation by plastic deformation are found, which is very significantly different when compared to Figure 8b. However, the formation of new grains in SZ is attributed to the strong plastic deformation that is generated by tool stirring and the heat generated by the friction of the tool, which promotes the recrystallization process in SZ.

4.6 Distribution of hardness for the butt welds

Table 2 shows the results of the 18 experiments, where the average value of the 18 tests was 83.47 ± 10.32 HV, and the fluctuation range of microhardness was not much. The average hardness value of the 12th set was the lowest at 75.95 HV, while the average hardness value of the 13th set was the highest at 99.9 HV. However, there is no significant change in the range of hardness in the whole 18 tests, and the trend remains consistent with the other tests, in which the hardness distribution is arranged in the order of parent material, heat-affected zone (HAZ), and weld zone. The hardness distribution of the welds is shown in Figure 9a. The shape of the curves in the 18 experiments is similar, almost like a W-profile, which is typical for all heat-treatable aluminum alloys. It is clear that there are four regions with different characteristics of microhardness, divided by black dashed lines. The four different regions, namely, SZ, HAZ, base metal (BM), and the narrow transition zone of TMAZ, are easily detected photographically in Figure 9a. There is, however, a degree of difference between the appearance of the weld beads with different parameters and the profile of the base material. The average hardness values of the nugget zone of the butt weld are about 70–75 HV. The core hardness falls within a distance equivalent to the radius of the stirring tool (4–8 mm) from the center line of the weld, which is mainly on the SZ side of the weld. This effect originates from the higher temperature and heating of the material in the SZ case, which generates a larger material overaging effect that leads to a decrease in hardness. The SZ has a lower hardness value than the BM. The hardness values of the SZ and TMAZ are almost the same for each sample. As can be seen in Figure 9a, the hardness value of the stirring zone slowly decreases from the HAZ to the SZ. A typical hardness profile shows that the minimum hardness is in the TMAZ zone. This is due to the process of the aging and annealing. As shown in the cross-sections of Figure 7b–e, based on the microhardness distribution of Figure 9a, the microstructures of BM, HAZ, TMAZ, and SZ of the welded bead are shown in SEM. As shown in Figure 9b, the crystallized grain structure and the evenly distributed particles can be clearly seen in the SM. From the grain observation, the initial grain microstructure of BM is still visible on the left side of HAZ in Figure 9c. The effect of FSW on the grain structure of HAZ is small. As shown in Figure 9c, some minor changes in grain size occur in the HAZ, while the size of the grains gradually becomes larger in the TMAZ. The TMAZ in Figure 7d has somewhat elongated grains and the grain size is close to that of SZ, and the microstructures of fine recrystallized and equiaxed grains can be also observed. The upper-left corner in Figure 9d shows that the grains of TMAZ are elongated at the interface near the SZ, while the TMAZ is close to the HAZ zone in the bottom of the right side, where a small amount of plastic deformation occurs in the recrystallized grains. Besides, in case of TMAZ, some elongated grains can be seen, while in SZ, these grains are much more prominent. As shown in Figure 9e, in SZ, due to the local deformation of the material in the heated zone, which is created by the rotating pin, it can promote an increase in the area of stirring and plastic deformation, which can be realized at higher temperatures. A higher degree of overaging is induced, which leads to much lower hardness values in SZ. That is, the recrystallization of the SZ caused by severe shear deformation and the large amount of heat generated during FSW resulting in elongated grains in the SZ. Due to the fact that 6061 aluminum alloy is a precipitation-reinforced alloy, the heat generated by friction leads to the reinforced precipitates (Mg_2Si, $MgZn_2$) of the aluminum alloy, which are easily dissolved or grown, resulting in the hardness value of the welded area being lower than that of the base material [16]. However, a W-type hardness distribution was observed in all cases, but due to the different cooling rates of the weld beads, microstructures were found to differ significantly leading to the differences in hardness.

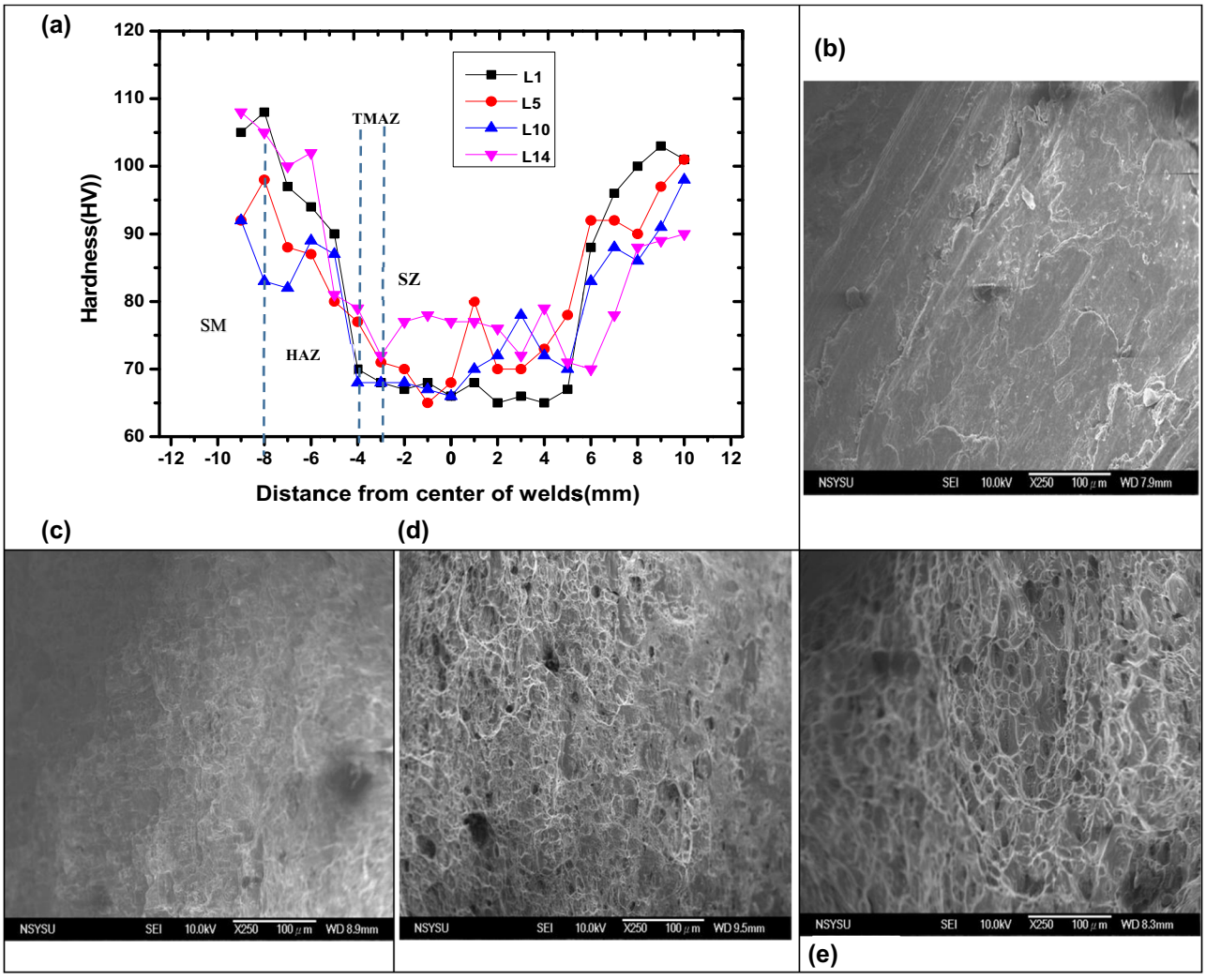

Figure 9: Hardness measurement is done at the middle line of the butt welds (a), the microstructure of the different zones for weld beads such as (b) SM, (c) HAZ, (d) TMAZ, and (e) SZ by FSW.

4.7 Distribution of impact strength

From the results of the 18 sets of experiments shown in Table 2, the impact strength (impact absorbed energy) of the 11th, 13th, and 16th sets was lower, with the 13th set at 8.66 $MJ{\cdot}m^{-2}$ being the lowest, and the 6th, 8th, and 17th sets had higher impact strengths, with the 6th set at 54.21 $MJ{\cdot}m^{-2}$ being the highest. As shown in Figure 7, the specimens in the 11th, 13th, and 16th sets were failed to bear the impact force that led to fracture from the weld zone, while the specimens in the 6th, 8th, and 17th sets showed that they only suffered bending deformation but did not fracture after the impact test. By extracting two groups from the previously described data in Table 2, the macroscopic and microscopic structures of the welded specimens in the impact test are further observed, as shown in Figure 10.

The impacting macrophotograph of the 13th set is shown in Figure 10a. A complete fracture pattern was detected in the stir-welded area with irregularities, which penetrated from the top to the bottom of the specimen, as well as large wrinkles and peeling fractures near the upper contact area of the specimen. It can be noted that TMAZ is weaker, which leads to the fracture of the welded area by the impacting load. On the other hand, as shown in Figure 10b, the defects found in the SEM have coarse grains and large voids, oxide contamination, and a lot of undulations in the region of the cracking scars. By comparison with Figure 10a, there is a bright white zone in the area of stir welding in Figure 10c, which is detected in the macroscopic pattern by the impacting force, and the bright white zone gradually expands from the top to the bottom of the specimen. No fracture sign was found in the stir-welding area

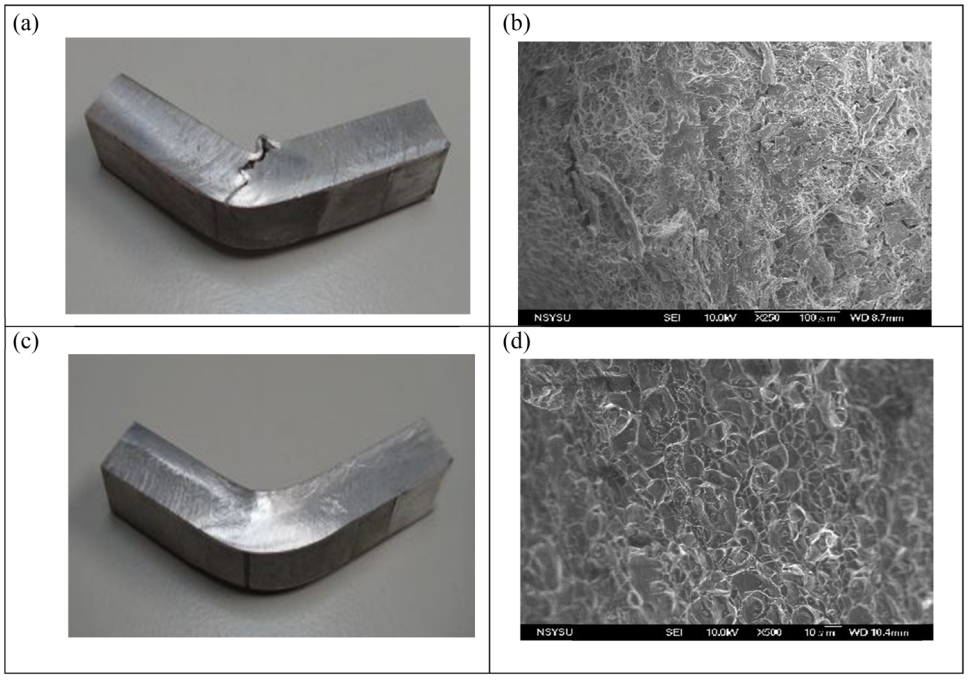

Figure 10: Macroscopic and microscopic structures with (a and b) test 13 and (c and d) test 6 of the welded specimens in the impact test.

of the specimen, which has a high impact resistance. Meanwhile, as shown in Figure 10d, the smooth and uniform structure of the impact pattern can be detected by SEM. While some grain growth was observed within the weld, limited defects were induced. It is evident that the fully recrystallized grains and structure of this weld when compared to Figure 10b were found to be extremely different. However, a clear difference between test 6 and test 13 can be seen. This difference is due to the variations in grain size, orientation, and the direction of flow.

4.8 Verification experiments

Based on the factorial effects in the response and variance tables, it can be seen that the best sets of parameters for multiple responses are in terms of A_1, B_3, C_3, D_3, E_2, F_1, G_2, and H_3. In addition, a validation experiment was performed to confirm the obtained responses. The four quality characteristics, namely, tensile, bending, impacting, and hardness, were normalized by grey relation grade and then formed into a fuzzy inference engine by "IF-THEN" rules. In this experiment, a fuzzy-grey synthesis algorithm with optimal stirring parameters based on Taguchi's design was used. Table 6 displays the results of the confirmed experiments. By comparing with the better tests in Table 2 and the initial test, it can be noted that the S/N ratio is −4.023, −1.002, and −0.721 dB, respectively. The S/N ratio of the optimal setting is the best among all 18 groups of tests. In addition, the individual properties of multiple responses such as tensile increased by 113.87%, bending increased by 137.86%, impacting increased by 139.87%, and hardness increased by 6.58% than the initial test. The overall improvement was 82.07%. Besides, the experimental results confirmed that the properties in terms

Table 6: Confirmation test for multiple response characteristics, including tensile, bending, impacting, and hardness data

Multi-response properties	Initial tests $A_1B_1C_1D_1E_1F_1G_1H_1$	Best test based on orthogonal array $A_2B_3C_2D_1E_3F_1G_2H_3$	Optimal test $A_1B_3C_3D_3E_2F_1G_2H_3$
Tensile strength (MPa)	91.33 ± 5.033	172.33 ± 2.082	195.33 ± 6.08/0.912
Bending strength (MPa)	22.42 ± 0.276	52.33 ± 0.577	53.33 ± 3.06/0.957
Impact strength ($MJ·m^{-2}$)	22.67 ± 2.887	53.81 ± 2.114	54.38 ± 1.36/0.996
Microhardness (HV)	79.05 ± 10.08	84.03 ± 15.10	84.25 ± 6.46/0.953
MPCI/S/N ratio of MPCI (dB)	0.396/−4.023	0.794/−1.002	0.847/−0.721

of tensile, bending, impact, and hardness values were 195.33 MPa, 53.33 MPa, 53.91 $J \cdot m^{-2}$, and 84.25 HV, respectively. The individual properties were increased by 13.35, 1.91, 1.05, and 0.26% as compared to the best test in all 18 groups. The overall performance increased by 28.04%. In total, it has successfully demonstrated the validity of the fuzzy-grey predictions based on Taguchi's design when applied to the multi-response performances of the FSW process. In other words, it is clear that the optimal factor for this model can yield a high-quality weld that is also sufficiently robust against noise effects to give better reproducibility.

5 Concluding remarks

The study incorporates a fuzzy logic based on grey system using Taguchi's design, which enables a full understanding of the characteristics of the individual and multiple responses of the beads of the joints in the FSW. It provides a new approach to solving ambiguous problems, which can be robustly solved using fuzzy-grey systems. Based on ANOVA, the effects of pin length, dwell time, tool rotational speed, and traverse speed on the multiple response of the weld are very significant, whereas the effects of backing plate, pin material, pin profile, and tilt angle are less significant. These significant factors accounted for almost 90.42% of the experimental variation. The experimental results showed the optimization of parameters of multiple responses in FSW, which allowed maximal tensile, bending, impacting, and suitable hardness to be obtained individually or simultaneously. This is a 28.04% increase in overall performance, while individual performance increases by 13.35, 1.91, 1.06, and 0.26%, respectively, when compared to the best results of all 18 groups. Based on experimental confirmation tests, this suggests a promising consistence between model predictions and experimental results. Accordingly, the proposed method can effectively evaluate the performance of multiple responses and individual weld quality, which can be used to enhance the welding performance of FSW. In total, it has successfully demonstrated the validity of the fuzzy-grey predictions based on Taguchi's design when applied to the multi-response performances of the FSW process.

Acknowledgements: The authors gratefully acknowledge financial support from the Project of Science and Technology Department of Fujian Province (No. KL5022006), Project of Educational Teaching Reform of Fujian Province (No.C150825), Undergraduate Education and Teaching Reform Research Project of Fujian Province (No. FBJG20220194), and the Industry-University Cooperative Education Projects of the Ministry of Education (No.202102100020; No.20210 2391031).

Funding information: This work was supported by the Project of Science and Technology Department of Fujian Province (KL5022006), Project of Educational Teaching Reform of Fujian Province (C150825), and Undergraduate Education and Teaching Reform Research Project of Fujian Province (FBJG20220194).

Author contributions: Yingjiao Chen: revision and funding; Mingder Jean: Writing, revision.

Conflict of interest: The authors state no conflict of interest.

Data availability statement: All authors can confirm that all data used in this article can be published the Journal "High Temperature Materials and Processes."

References

[1] Kumbhar, N. T. and K. Bhanumurthy. Friction stir welding of A1 6061 alloy. *Asian Journal of Experimental Sciences*, Vol. 22, No. 2, 2008, pp. 63–74.
[2] Mishra, R. S. and Z. Y. Ma. Friction stir welding and processing. *Materials Science and Engineering: R*, Vol. 50, No. 1–2, 2005, pp. 1–78.
[3] Ma, Z. Y. Friction stir processing technology: A review. *Metallurgical and Materials Transactions A*, Vol. 39, 2008, pp. 642–658.
[4] Huang, G. and S. Kouc. Partially melted zone in aluminum welds - liquation mechanism and directional solidification. *Welding Research*, Vol. 5, No. Supplement, 2000, pp. 113–120.
[5] Rhodes, C. G., M. W. Mahoney, W. H. Bingel, R. A. Spurling, and C. C. Bampton. Effects of friction stir welding on microstructure of 7075 aluminum. *Scripta Materialia*, Vol. 36, No. 1, 1997, pp. 69–75.
[6] Jin, H., S. Saimoto, M. Ball, and P. L. Threadgill. Characterisation of microstructure and texture in friction stir welded joints of 5754 and 5182 aluminium alloy sheets. *Materials Science and Technology*, Vol. 17, No. 12, 2001, pp. 1605–1614.
[7] Sato, Y. S., M. Urata, H. Kokawa, and K. Ikeda. Hall–Petch relationship in friction stir welds of equal channel angular-pressed aluminium alloys. *Materials Science and Engineering: A*, Vol. 354, No. 1–2, 2003, pp. 298–305.
[8] Thomas, W. M., P. L. Threadgill, and E. D. Nicholas. Feasibility of friction stir welding steel. *Science and Technology of Welding and Joining*, Vol. 4, No. 6, 1999, pp. 365–372.
[9] Li, Y., L. E. Murr, and J. C. McClure. Flow visualization and residual microstructures associated with the friction-stir welding of 2024 aluminum to 6061 aluminum. *Materials Science and Engineering: A*, Vol. 271, No. 1–2, 1999, pp. 213–223.
[10] Sato, Y. S., F. Yamashita, Y. Sugiura, S. H. C. Park, and H. Kokawa. FIB-assisted TEM study of an oxide array in the root of a friction stir welded aluminium alloy. *Scripta Materialia*, Vol. 50, No. 3, 2004, pp. 365–369.
[11] Srivatsan, T. S., S. Vasudevan, and L. Park. The tensile deformation and fracture behavior of friction stir welded aluminum alloy 2024.

Materials Science and Engineering: A, Vol. 466, No. 1–2, 2007, pp. 235–245.

[12] Liu, H., H. Fujii, M. Maeda, and K. Nogi. Tensile properties and fracture locations of friction-stir welded joints of 6061-T6 aluminum alloy. *Journal of Materials Science Letters*, Vol. 22, 2003, pp. 1061–1063.

[13] Barcellona, A., G. Buffa, L. Fratini, and D. Palmeri. On microstructural phenomena occurring in friction stir welding of aluminium alloys. *Journal of Materials Processing Technology*, Vol. 177, 2006, pp. 340–343.

[14] Lee, W. B. and S. B. Jung. The joint properties of copper by friction stir welding. *Materials Letters*, Vol. 58, No. 6, 2004, pp. 1041–1046.

[15] Liu, G., L. E. Murr, C. S. Niou, J. C. McClure, and F. R. Vega. Microstructural aspects of the friction-stir welding of 6061-T6 aluminum. *Scripta Materialia*, Vol. 37, No. 3, 1997, pp. 355–361.

[16] Krishnan, K. N. The effect of post weld heat treatment on the properties of 6061 friction stir welded joints. *Journal of Materials Science*, Vol. 37, 2002, pp. 473–480.

[17] Chen, H. B., K. Yan, T. Lin, S. B. Chen, C. Y. Jiang, and Y. Zhao. The investigation of typical welding defects for 5456 aluminum alloy friction stir welds. *Materials Science and Engineering: A*, Vol. 433, No. 1–2, 2006, pp. 64–69.

[18] Krishnan, K. N. On the formation of onion rings in friction stir welds. *Materials Science and Engineering: A*, Vol. 327, No. 2, 2002, pp. 246–251.

[19] Lim, S., S. Kim, C. G. Lee, and S. Kim. Tensile behavior of friction-stri-welded Al 6061-T651. *Metallurgical and Materials Transactions A*, Vol. 35, 2004, pp. 2829–2835.

[20] Liu, H., M. Maeda, H. Fujii, and K. Nogi. Tensile properties and fracture locations of friction-stir welded joints of 1050-H24 aluminum alloy. *Journal of Materials Science Letters*, Vol. 22, 2003, pp. 41–43.

[21] Lee, W. B., Y. M. Yeon, and S. B. Jung. Mechanical properties related to microstructural variation of 6061 Al alloy joints by friction stir welding. *Materials Transactions*, Vol. 45, No. 5, 2004, pp. 1700–1705.

[22] Zadpoor, A. A., J. Sinke, R. Benedictus, and R. Pieters. Mechanical properties and microstructure of friction stir welded tailor-made blanks. *Materials Science and Engineering: A*, Vol. 494, No. 1–2, 2008, pp. 281–290.

[23] Ramulu, P. J., R. G. Narayanan, S. V. Kailas, and J. Reddy. Internal defect and process parameter analysis during friction stir welding of Al 6061 sheets. *The International Journal of Advanced Manufacturing Technology*, Vol. 65, 2013, pp. 1515–1528.

[24] Ghosh, M., K. Kumar, S. V. Kailas, and A. K. Ray. Optimization of friction stir welding parameters for dissimilar aluminum alloys. *Materials & Design*, Vol. 31, No. 6, 2010, pp. 3033–3037.

[25] Rajakumar, S. and V. Balasubramanian. Establishing relationships between mechanical properties of aluminium alloys and optimised friction stir welding process parameters. *Materials & Design*, Vol. 40, 2012, pp. 17–35.

[26] Kamp, N., A. P. Reynolds, and J. D. Robson. Modelling of 7050 aluminium alloy friction stir welding. *Science and Technology of Welding and Joining*, Vol. 14, No. 7, 2009, pp. 589–596.

[27] Rajakumar, S., C. Muralidharan, and V. Balasubramanian. Predicting tensile strength, hardness and corrosion rate of friction stir welded AA6061-T6 aluminium alloy joints. *Materials & Design*, Vol. 32, No. 5, 2011, pp. 2878–2890.

[28] Bozkurt, Y. and M. K. Bilici. Application of Taguchi approach to optimize of FSSW parameters on joint properties of dissimilar AA2024-T3 and AA5754-H22 aluminum alloys. *Materials & Design*, Vol. 51, 2013, pp. 513–521.

[29] Patel, N. P., P. Parlikar, R. S. Dhari, K. Mehta, and M. Pandya. Numerical modelling on cooling assisted friction stir welding of dissimilar Al-Cu joint. *Journal of Manufacturing Processes*, Vol. 47, 2019, pp. 98–109.

[30] Elangovan, K. and V. Balasubramanian. Influences of pin profile and rotational speed of the tool on the formation of friction stir processing zone in AA2219 aluminium alloy. *Materials Science and Engineering: A*, Vol. 459, No. 1–2, 2007, pp. 7–18.

[31] Bayazid, S., H. Farhangi, and A. Ghahramani. Investigation of friction stir welding parameters of 6063-7075 aluminum alloys by Taguchi method. *Procedia Materials Science*, Vol. 11, 2015, pp. 6–11.

[32] Kadaganchi, R., M. R. Gankidi, and H. Gokhale. Optimization of process parameters of aluminum alloy AA 2014-T6 friction stir welds by response surface methodology. *Defence Technology*, Vol. 11, 2015, pp. 209–219.

[33] Raja, A. R., M. Vashista, and M. Z. K. Yusufzai. Estimation of material properties using hysteresis loop analysis in friction stir welded steel plate. *Journal of Alloys and Compounds*, Vol. 814, 2020, id. 152265.

[34] Zhang, H. J., H. J. Liu, J. L. Song, Q. L. Guan, and Z. J. Ji. Microcharacteristic and formation mechanism of layered band structure in non-weld-thinning friction stir welded 7N01 aluminum alloy. *Journal of Manufacturing Processes*, Vol. 50, 2020, pp. 154–160.

[35] Sunilkumar, D., S. Muthukumaran, M. Vasudevan, and M. Reddy. Tool rotational speed variant response on the evolution of microstructure and its significance on mechanical properties of friction stir welded 9Cr-1Mo steel. *Journal of Materials Processing Technology*, Vol. 278, 2020, id. 116536.

[36] Li, N., Y. J. Chen, and D. D. Kong. Multi-response optimization of Ti-6Al-4V turning operations using Taguchi-based grey relational analysis coupled with kernel principal component analysis. *Advances in Manufacturing*, Vol. 7, 2019, pp. 142–154.

[37] Meng, X., Y. Huang, J. Cao, J. Shen, and J. F. dos Santos. Recent progress on control strategies for inherent issues in friction stir welding. *Progress in Materials Science*, Vol. 115, 2021, id. 100706.

[38] Soori, M., M. Asmael, and D. Solyalı. Recent development in friction stir welding process. *SAE International Journal of Materials and Manufacturing*, Vol. 14, No. 1, 2021, pp. 63–80.

[39] Mehta, K. P., P. Carlone, A. Astarita, F. Scherillo, F. Rubino, and P. Vora. Conventional and cooling assisted friction stir welding of AA6061 and AZ31B alloys. *Materials Science and Engineering: A*, Vol. 759, 2019, pp. 252–261.

[40] Chen, G., S. Zhang, Y. Zhu, C. Yang, and Q. Shi. Thermo-mechanical analysis of friction stir welding: A review on recent advances. *Acta Metallurgica Sinica (English Letters)*, Vol. 33, 2020, pp. 3–12.

[41] Hou, W., L. H. A. Shah, G. Huang, Y. Shen, and A. Gerlich. The role of tool offset on the microstructure and mechanical properties of Al/Cu friction stir welded joints. *Journal of Alloys and Compounds*, Vol. 825, 2020, id. 154045.

[42] Shaik B, Harinath Gowd G, and Durga Prasad B. Investigations and optimization of friction stir welding process to improve microstructures of aluminum alloys. *Cogent Engineering*, Vol. 6, No. 1, 2019, pp. 1–14.

[43] Jain S, Sharma N, Gupta R. Dissimilar alloys (AA6082/AA5083) joining by FSW and parametric optimization, using Taguchi, grey relational and weight method. *Engineering Solid Mechanics*, Vol. 6, No. 1, 2018, pp. 51–66.

[44] Jagadish, S. Bhowmik, and A. Ray. Development of fuzzy logic-based decision support system for multi-response parameter optimization of green manufacturing process: A case study. *Soft Computing*, Vol. 23, 2019, pp. 11015–11034.
[45] Vijayan, S. Multi objective optimization of friction stir welding process parameters on aluminum alloy AA 5083 using taguchi based grey relation analysis. *Materials and Manufacturing Processes*, Vol. 25, 2010, pp. 1206–1212.
[46] Venkateswarlu, D., P. Nageswara Rao, M. M. Mahapatra, S. P. Harsha, and N. R Mandal. Processing and optimization of dissimilar friction stir welding of AA 2219 and AA 7039 alloys. *Journal of Materials Engineering and Performance*, Vol. 24, 2015, pp. 4809–4824.
[47] Senthil, S. M., R. Parameshwaran, S. Ragu Nathan, M. Bhuvanesh Kumar, and K. Deepandurai. A multi-objective optimization of the friction stir welding process using RSM-based-desirability function approach for joining aluminum alloy 6063-T6 pipes. *Structural and Multidisciplinary Optimization*, Vol. 62, 2020, pp. 1117–1133.
[48] Ojo, O. O. and E. Taban. Hybrid multi-response optimization of friction stir spot welds: failure load, effective bonded size and flash volume as responses. *Sadhana Academy Proceedings in Engineering Sciences*, Vol. 43, 2018, pp. 98–112.
[49] Puviyarasan, M. and V. S. Senthil Kumar. An experimental investigation for multi-response optimization of friction stir process parameters during fabrication of AA6061/B4Cp composites. *Arabian Journal for Science and Engineering*, Vol. 40, 2015, pp. 1733–1741.
[50] Dinesh Kumar, R., M. S. Ilhar Ul Hassan, S. Muthukumaran, T. Venkateswaran, and D. Sivakumar. Single and multi-response optimization and validation of mechanical properties in dissimilar friction stir welded AA2219-T87 and AA7075-T73 alloys using T-GRA. *Experimental Techniques*, Vol. 43, 2019, pp. 245–259.
[51] Guan, W., Y. Zhao, Y. Liu, S. Kang, D. Wang, and L. Cui. Force data-driven machine learning for defects in friction stir welding. *Scripta Materialia*, Vol. 217, 2022, id. 114765.
[52] Sudhagar, S., M. Sakthivel, and P. Ganeshkumar. Monitoring of friction stir welding based on vision system coupled with Machine learning algorithm. *Measurement*, Vol. 144, 2019, pp. 135–143.
[53] Ramamurthy, M., P. Balasubramanian, N. Senthilkumar, and G. Anbuchezhiyan. Influence of process parameters on the microstructure and mechanical properties of friction stir welds of AA2014 and AA6063 aluminium alloys using response surface methodology. *Materials Research Express*, Vol. 9, No. 2, 2022, id. 026528.
[54] Zhang, C. Y., Q. D. Chen, and M. D. Jean. Optimization of the welding properties of friction stir butt joints by using RSM based on Taguchi design. *Strength of Materials*, Vol. 54, No. 2, 2022, pp. 267–280.
[55] Sevvel, P., C. Satheesh, and R. Senthil Kumar. Generation of regression models and multi-response optimization of friction stir welding technique parameters during the fabrication of AZ80A Mg alloy joints. *Transactions of the Canadian Society for Mechanical Engineering*, Vol. 44, No. 2, 2019, pp. 311–324.
[56] Rathinasuriyan, C. and V. S. Kumar. Optimisation of submerged friction stir welding parameters of aluminium alloy using RSM and GRA. *Advances in Materials and Processing Technologies*, Vol. 7, No. 4, 2021, pp. 696–709.
[57] Sharma, N., Z. A. Khan, A. N. Siddiquee, and M. A. Wahid. Multi-response optimization of friction stir welding process parameters for dissimilar joining of Al6101 to pure copper using standard deviation based TOPSIS method. *Proceedings of the Institution of Mechanical Engineers, Part C: Journal of Mechanical Engineering Science*, Vol. 233, No. 18, 2019, pp. 6473–6482.
[58] Sefene, E. M. and A. A. Tsegaw. Temperature-based optimization of friction stir welding of AA 6061 using GRA synchronous with Taguchi method. *The International Journal of Advanced Manufacturing Technology*, Vol. 119, 2022, pp. 1479–1490.
[59] Chanakyan, C., S. Sivasankar, M. Meignanamoorthy, and S. V. Alagarsamy. Parametric optimization of mechanical properties via FSW on AA5052 using Taguchi based grey relational analysis. *Incas Bulletin*, Vol. 13, No. 2, 2021, pp. 21–30.
[60] Jambhale, S., S. Kumar, and S. Kumar. Multi-response optimization of friction stir spot welded joint with grey relational analysis. *Materials Today: Proceedings*, Vol. 27, 2020, pp. 1900–1908.
[61] Dikshit, M. K., V. K. Pathak, B. Bhavani, M. K. Agrawal, V. Malik, and A. Saxena. Optimization of cutting forces in high-speed ball-end milling using fuzzy-based desirability function approach. *International Journal on Interactive Design and Manufacturing*, 2023, pp. 1–14.
[62] Sharma, S., D. Anitha, V. Chaturvedi, J. Vimal, P. Jayaswal, and K. K. Saxena, et al. MIG welding process parameter optimisation of AISI 1026 steel using Taguchi-TOPSIS method. *International Journal on Interactive Design and Manufacturing*, 2023, pp. 1–13.
[63] Ross, P. J. *Taguchi techniques for quality engineering*, Tata McGraw-Hill Publishing Company Limited, New Delhi, 2008.
[64] Deng, J. L. Introduction to grey system theory. *Journal of Grey System*, Vol. 1, No. 1, 1989, pp. 1–24.
[65] Ross, T. *Fuzzy logic with engineering application*, McGraw-Hill, New York, 1995.